CHAPTER 28

SIMULATION OF HORIZONTAL TURBULENT DIFFUSION OF PARTICLES UNDER WAVES

By Stephen P. Murray
Coastal Studies Institute
Louisiana State University
Baton Rouge, Louisiana

ABSTRACT

By oscillation of an array of turbulence-generating grids in still water, the turbulent fluid velocity field in shoaling waves near the bottom is simulated in a laboratory channel. Solid particles with fall velocities varying between 1 and 40 mm/sec are introduced into the test volume from above. Multiple-image photography using ultraviolet lighting techniques and a suitably placed mirror allow recording of the grain trajectories as functions of time and three space dimensions simultaneously. The Lagrangian intensities of turbulence and diffusion coefficients are then directly measured from the photographic data. The scale times, scale lengths, and the frequencies of the power spectra modes can then be calculated. Properties of the fluid turbulence are inferred from the quasi-neutral particles. The analysis, which is restricted to the component of diffusion in the horizontal direction normal to the grid motion, shows that the turbulent velocity distributions of both fluid and heavy particles are Gaussian, and that their standard deviations (intensities of turbulence) increase regularly with increasing grid Reynolds numbers (grid speeds). Diffusion coefficients likewise generally increase with increasing grid Reynolds numbers. Diffusivities of the heavy particles relative to the fluid are a function of both particle fall velocity and the structure of the fluid turbulence itself.

I. INTRODUCTION

With the advent of fluorescent sand tracers in the marine environment, much attention has recently been focused on the dispersion of solid particles by waves. In this regard, studies by Bowen and Inman (1966) and Murray (1967) suggest that the role of turbulent diffusion must be investigated. The basic aims of this study, therefore, are (1) to determine the effect of increasing terminal fall velocity on the turbulent diffusion of solid particles inside shallow-water waves, (2) to investigate the applicability of the statistical theory of turbulence to heavy particles, and (3) to compare the internal properties of the fluid and particle turbulence.

In unidirectional flow the mean velocity in any direction k is generally defined by

$$\bar{u}_k \equiv \frac{1}{T} \int_{t_o-1/2T}^{t_o+1/2\ T} u_k \, dt, \qquad (1)$$

where u_k is the velocity at any instant and T is taken sufficiently long to yield a stable average. The difference between u_k and $\bar{u}_k$

$$u_k' = u_k - \bar{u}_k \tag{2}$$

is referred to as the turbulent velocity. In the case of the periodically varying velocities within waves it is less evident how to define mathematically the average and turbulent terms. Knowledge of turbulence in waves is scant. Stewart and Grant (1962) measured the turbulent energy spectra in the presence of surface waves and illustrated a low-frequency peak attributed to orbital motions. Perhaps turbulence in waves can be defined in terms of such deviations in the energy spectra. In any case, the flow in nature is clearly not laminar, and a turbulence term must exist which in turn gives rise to the diffusion effects which are the basic aim of this study.

The complexities of the problem demand an experimental approach, and, since the available wave tank was not of sufficient size to generate fully turbulent waves, a simulation technique was devised. This technique consists essentially of oscillating an array of grids through still water in a sinusoidal manner. Variation of the grid oscillation speed allows the generation of several turbulent-flow fields. Fluorescent lighting techniques, combined with multiple-image photography, provide records of the coordinates of individual particles in time and three-dimensional space for further analysis. The experimental work, which was conducted in the Fluid Mechanics Laboratory of the Delft Technological University, the Netherlands, has direct implications on the dynamics of suspended sediment in the surf zone.

II. THEORETICAL CONSIDERATIONS

Of the several theories describing and predicting the turbulent spreading of a collection of particles, the "single particle" theory of G. I. Taylor (1921, 1935) offers the best framework for the present study. Taylor expressed particle displacement caused by turbulence x_k' as a time-integrated effect of the turbulent velocity u_k'

$$x_k' = \int_o^t u_k'(t)\, dt. \tag{3}$$

Considering a collection of many particles and taking the mean square of all such net displacements as the appropriate statistical measure of the particle dispersion yields the Taylor diffusion equation

$$\sigma_k^2(T) = 2\,\overline{u_k'^2} \int_o^T \int_o^t R_k(\xi)\, d\xi\, dt. \tag{4}$$

Here σ_k^2 is the variance of the displacements of the particles from their initial position, $\left(\overline{u_k'^2}\right)$ is the square of the turbulence intensity--alternatively known as the root mean square turbulent velocity--which should be approximately constant in a given flow field, R_k is the Lagrangian autocorrelation function of the velocity, and ξ is the autocorrelation lag time. The subscript k refers

to any direction and (4) applies equally to the x, y, or z direction when only turbulent motions are present with the corresponding velocities u', v', and w'. For a detailed derivation of (4) see Haltiner and Martin (1957, p. 276).

For large values of the lag time ξ the velocity autocorrelation $R_k(\xi)$ approaches zero and the area c under the autocorrelation function versus time curve--that is, the inner integral of (4)--becomes constant

$$\int_0^\infty R_k(\xi)\, d\xi = c_k. \tag{5}$$

Henceforth all equations will be written in the y direction. Performing the second integration of (4) leads to

$$\sigma_y^2(T) = 2\,\overline{v'^2}\, c_y T. \tag{6}$$

Taking the first derivative of (6)

$$\frac{d\sigma_y^2}{dT} = 2\,\overline{v'^2}\, c_y, \tag{7}$$

which shows that, for long elapsed diffusion times, the slope of the $\sigma^2 - T$ curve is a constant, a result we shall use later. For very short diffusion times the autocorrelation is unity and (4) reduces to

$$\sigma_y^2 = \overline{v'^2}\, T^2. \tag{8}$$

This equation applies only up to about .04 seconds, as deduced from Frenzen's results (1963) under conditions similar to ours. The resolution of our data is insufficient for (8) to be of any use. The area under the Lagrangian autocorrelation coefficient is generally referred to as the scale time of the turbulence, denoted by t_y^* (9),

$$t_y^* \equiv c_y, \tag{9}$$

$$\ell_y^* = \left(\overline{v'^2}\right)_y^{1/2} t_y^*, \tag{10}$$

$$K_y^* = 1/2\left(\frac{d\sigma_y^2}{dT}\right) = \left(\overline{v'^2}\right)_y t_y^* = \left(\overline{v'^2}\right)^{1/2} \ell_y^*. \tag{11}$$

The scale time t_y^* can be considered to measure the lifetime of the largest turbulent cell (Inoue, 1960). The Lagrangian scale length ℓ_y^* (10) is usually interpreted as a measure of the average turbulent eddy size. It is analogous to the "mixing length" of Prandtl's earlier theory. The Lagrangian diffusion coefficient K_y^* is equal to one half the ultimate rate of particle spread (11), and using (7) and (10) it can be expressed in terms of the turbulence intensity, the scale time, and the scale length. In addition, t_y^* can be interpreted in terms of the distribution of energy in the Lagrangian power spectrum

through a Fourier cosine transform (Taylor, 1938). Frenzen (1963, p. 67) shows that the mode of the power spectrum n in cycles per second can be closely approximated by

$$n_y = 1/2\ (\pi t_y^*)^{-1}. \tag{12}$$

The complete integral solution of (4) requires knowledge of the form of the autocorrelation function $R_y(\xi)$. Inoue's theoretical analysis (1951) predicts the autocorrelation function to approximate the form

$$R_y(\xi) = \exp\ (-\xi/c_y), \tag{13}$$

which was verified experimentally by Kalinske and Pien (1944) and Frenzen (1963) for unstratified flows. Substituting (13) into (4) and integrating yields a general diffusion equation

$$\sigma_y^2 = 2\ \overline{v'^2}\ c_y\ T - 2\ \overline{v'^2}\ \ c_y^2 + 2\ \overline{v'^2}\ c_y^2\ \exp\ (-T/c_y), \tag{14}$$

showing that in a fluid velocity field composed only of turbulent motions the dispersion of a collection of particles is a function of the turbulence intensity, the elapsed diffusion time, and the scale time of the turbulence.

III. EXPERIMENTAL PROCEDURES

The use of turbulence-generating grids has yielded great advances in the knowledge of turbulence in air streams, but they have been used only rarely in hydrodynamics. The disturbances generated in the lee of a grid (with either the fluid or the grid in motion) has been shown by Taylor (1935) to transform rapidly into a quasi-isotropic turbulent field. For an excellent photograph of this phenomenon showing the initial vortices degenerating into a homogeneous turbulent field, see Prandtl (1939). Although it is well recognized that quasi-isotropic grid-produced turbulence only crudely resembles the turbulent shear flows of nature, its study has precipitated great progress in the understanding of the mechanics of turbulence itself. Frenzen (1963) describes detailed experiments in which a single grid is towed through a water channel so that the turbulent trajectories of particles may be studied without the disadvantage of a mean flow moving the particles rapidly out of the field of view. As a variation of Frenzen's technique, in this study a series of grids is oscillated in simple harmonic motion in still water.

To rationalize the analogy between turbulence in shallow-water waves and grid-produced turbulence, consider Figure 1. Diagram A of this figure shows the well known result that in idealized water waves to the first approximation the orbital velocity varies sinusoidally in time. If the wave flow were turbulent, the velocity trace would presumably resemble Figure 1 B, since the "turbulent fluctuations are approximately proportional to the mean velocity" (Sutton, 1953, p. 251). The elimination of the sinusoid from Figure 1 B represents a turbulence field (Fig. 1 C) without the

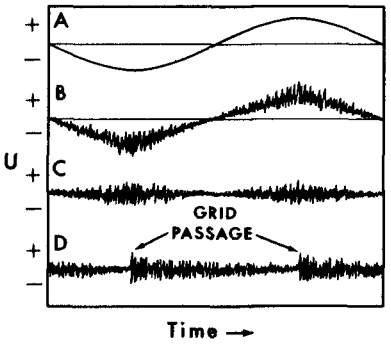

Fig. 1. Sketch to illustrate similarity of oscillating grid-produced turbulence to turbulent wave flow.

disturbance of orbital motions. The present experiments attempt to simulate Figure 1 C by sinusoidally oscillating a grid in still water. In Eulerian coordinates the turbulent velocity so produced (see Figure 1 D) will abruptly peak as the grid passes; this will be followed by a gradual decay until the next grid passage, and a crude approximation to the turbulence shown in diagram C will ensue. However, as will be shown later, the observed frequency distributions of the turbulent velocity are Gaussian in nature, so perhaps the results concerning the particle diffusion apply equally as well to turbulent fields in general. The laboratory flow is a simulation or model of turbulent wave flow in nature only in the sense of this paragraph.

The grids which fill the 50 cm wide channel are composed of steel rods 1 cm in diameter and 5 cm apart. The array, consisting of three grids, each 30 cm apart, has a stroke length kept constant at 40 cm. For the experiments average grid velocities of 16, 30, and 45 cm/sec are determined by variation of the oscillation period. The grid Reynolds number Re_g is defined by the mean fluid velocity $\bar{U}$, the grid mesh length M, and the kinematic viscosity of the fluid ν

$$Re_g = \frac{\bar{U}\, M}{\nu} \,. \tag{15}$$

With $\bar{U}$ considered as the average grid speed, (15) defines three grid Reynolds numbers: 0.66×10^4, 1.2×10^4, and 1.9×10^4. Water depth is kept constant at 40 cm. The elimination of data taken (a) within 5 cm of the walls because of boundary effects and (b) within the 10 cm section at each end of the grid stroke leaves an experimental volume inside the tank 80 cm long, 30 cm high, and 40 cm across.

In conventional studies of grid-produced turbulence a correction for the time decay of the turbulence is generally made. In this study a new burst of turbulence, associated with the oscillating grids, reinforces the velocity field every few seconds (cf. Fig. 1 D). The particle trajectories from which the data are taken encompass the entire volume and time duration of an experiment. Thus the trajectories are a direct result of several turbulent bursts, and their sampling (at 1-second intervals) is considered to produce an average which represents an effective turbulence field, no decay corrections being required.

As a means of observing particle diffusion, solid, wax-like particles

2 mm in diameter d are impregnated with a fluorescent powder and injected into the test volume from above. The density of such particles (diameter remains constant) can be varied to evaluate changes in the diffusion brought on by the terminal fall velocities. Repeated timing of the duration of fall through a column of water determines terminal fall velocities w_p of 0.2, 1.0, 2.0, 3.0, and 4.0 cm/sec. Table 1 lists the corresponding particle Reynolds numbers ($Re_p = w_p\, d/\nu$) and sedimentation diameters d_s--that is, the size of spherical quartz grains having the same fall velocities as our test particles (Brown, 1950). The 0.2 cm/sec particle is referred to as the fluid or quasi-neutral particle and is used to infer the statistics of the fluid turbulence.

Table 1

Properties of the Test Particles					
w_p cm/sec	0.2	1.0	2.0	3.0	4.0
Re_p	2.4	16.6	33.3	50.0	66.6
d_s (mm)	0.03	0.12	0.18	0.24	0.38

Two 500-watt mercury vapor lamps are directed diagonally down into the test volume to provide illumination of the fluorescent particles and several centimeter scales. The camera is situated 3 m in front of the water channel and aimed at the center of the front glass experimental area. A red filter on the lens insures that the only light to strike the 10 cm x 12 cm negative comes from the red-emitting objects treated with the fluorescent powder--that is, the particles and the centimeter scales. To achieve the multiple-image effect, a metal disc pierced with six holes along its periphery rotates in front of the camera lens. The holes act as a rapidly repeating camera shutter. In order to see both a front and a top view of the experimental volume simultaneously in the same photograph--that is, all three dimensions at once--a high-quality glass mirror is rigidly suspended over the channel. One essential feature of this photographic technique is that the grids are invisible to the camera.

Rouse (1939) describes a device used in a study of vertical particle diffusion which is mechanically similar to the one discussed above. Rouse calculated diffusion coefficients from the concentration statistics of a collection of particles.

IV. ANALYSIS AND RESULTS

Fifteen photographs (2 grain trajectories per photograph) were taken of each fall velocity at each grid Reynolds number. After development of the film 50 cm x 60 cm enlargements were made in the photographic laboratories of both the Delft Tecbnological University and the Coastal Studies Institute. Figure 2 is an example of one data-bearing photograph. The lower half is the front view, giving the x and z coordinates, z being the vertical direction; the upper half is the image in the mirror, giving the x and y coordinates, the y direction being across the channel width. In this photograph there are eighteen particle images per second, a fall

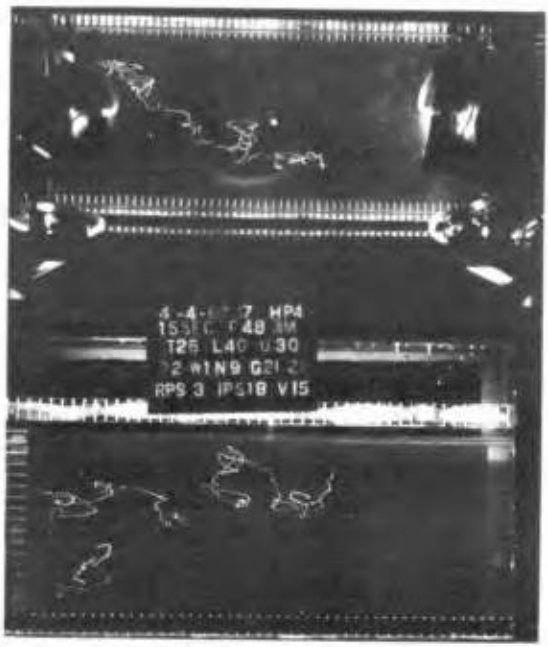

Fig. 2. Example of a data-bearing photograph; grid speed of 30 cm/sec, 18 images per second.

velocity of 0.2 cm/sec, and an average grid speed of 30 cm/sec. Four fall velocities are examined at the lowest value of Re_g and five, at the two higher. Thus there are fourteen data sets, each composed of thirty grain trajectories. The grains are followed in the x, y, and z directions for about 10 seconds.

Scale overlays are constructed to facilitate the reading of the particle coordinates from the photographs, and by counting the number of images we can tell the duration of elapsed time from the start of the trajectory. As a means of distinguishing the end of the trajectory from the beginning, the last few seconds of the photograph are made with the disc stopped and a hole directly in front of the lens so that the particle makes an easily distinguished continuous streak on the negative.

The x coordinate is common to both halves of the photograph, which helps in correlating the front and top views. With practice the paths of the particles can be followed in all three dimensions and time quite well. The particle coordinate is read each second up to 10 seconds for the data analysis. This sampling procedure controls the frequency band within which we are viewing the particle movements. For N observations taken ΔT seconds apart the spectral band we are viewing is given approximately by

$$\frac{1}{2N\Delta T} < f < \frac{1}{2\Delta T} , \qquad (16)$$

where f is the frequency in cycles per second. In the present experiments $\Delta T = 1$ second and $N = 10$, so our observations are restricted to the range between 0.05 and 0.5 cps.

Because of the proximity of the camera to the experimental tank there is a significant parallax error. A centered difference correction technique

is employed which reduces this error to at most 4 percent.

In the remainder of the paper discussion will be restricted to the component of diffusion in the y direction; that is, horizontal diffusion laterally across the channel, normal to the grid motion. The component of particle motion in the y direction is obtained simply by projecting the particle onto the y axis. In a sense we are then observing the particle moving back and forth along a single line--the y axis.

The particle motion along the x axis is difficult to interpret because of dragging effects of the grids. This is not a serious drawback, however, as the turbulence characteristics in any horizontal direction should be approximately the same in our simplified flow field; i.e., the x-direction data should approximate that of the y direction. The data on diffusion in the vertical (z) direction, including the interaction of turbulence and fall velocities, will be presented elsewhere. The three-dimensional value of any of the turbulence parameters can be obtained, if desired, by calculation of the resultant vector.

Particle Spread

We now have the particle coordinates as a function of time. In order to utilize equation (6), we calculate the variance (σ_y^2) of particle displacements from the initial position for each 1-second time increment using

$$\sigma_y^2 (T) = \sum_1^n \frac{(y_i - y_o)^2}{n} , \tag{17}$$

where n refers to the number of particles, y_o to the initial and y_i to the subsequent coordinates. Unlike the more conventional mean, y_o will vary with each particle, but in a field of homogeneous turbulence this is inconsequential. A plot of σ_y^2 against time T should then, from (7), become linear after a few seconds, with the slope equal to twice the product of the turbulence intensity (squared) and the scale time; or, alternatively, the diffusion coefficient is equal to one half of this slope (see equation 11). In practice we calculate the slope of the least squares regression line passing through the points for $t \geq 2$ sec. These slopes, together with the corresponding correlation coefficients r, are presented in Table 2.

The uniformly high values of the correlation coefficients indicate the linear spread law holds valid after 2 seconds in our experiments for both the fluid and the heavy particles at all values of Re_g.

Turbulent Velocities

The data on the time change of the particle coordinates also allow measurement of the turbulent velocities v' from

$$v' = \frac{y(t) - y(\Delta t)}{\Delta t} . \tag{18}$$

Table 2
Ultimate Slope of Dispersion Curves

Re_g	0.66×10^4			
w_p (cm/sec)	0.2	1.0	2.0	3.0
$\frac{d\sigma^2}{dT} = 2K^*$ (cm^2/sec)	8.8	4.8	5.0	4.4
r	.98	.96	.99	.98

Re_g	1.2×10^4				
w_p (cm/sec)	.2	1.0	2.0	3.0	4.0
$\frac{d\sigma^2}{dT} = 2K^*$ (cm^2/sec)	7.6	18	16	7.4	9.5
r	.89	.99	.98	.93	.94

Re_g	1.9×10^4				
w_p (cm/sec)	.2	1.0	2.0	3.0	4.0
$\frac{d\sigma^2}{dT} = 2K^*$ (cm^2/sec)	25	22	18	14	22
r	.96	.98	.99	.97	.97

Since Δt = 1 second the difference in successive particle coordinates is a direct measurement of the turbulent velocity. In a given data set there are thirty particles followed for 5 to 10 seconds, resulting in about 200 measurements of the turbulent velocity per data set. Percent distribution (histograms) of turbulent velocities and corresponding Gaussian curves of best fit are plotted in Figure 3, where N is the number of observations. At this point there are three notation changes:

1. We shall use the notation $\underline{v}'$ for the intensity of turbulence; that is, $\underline{v}' \equiv (\overline{v'^2})^{1/2}$;

2. The subscript o, e.g., $\underline{v}'_o$, refers to a property of the fluid, the subscript p refers to a property of a heavy particle, e.g., $\underline{v}'_p$, lack of a subscript refers to both phases;

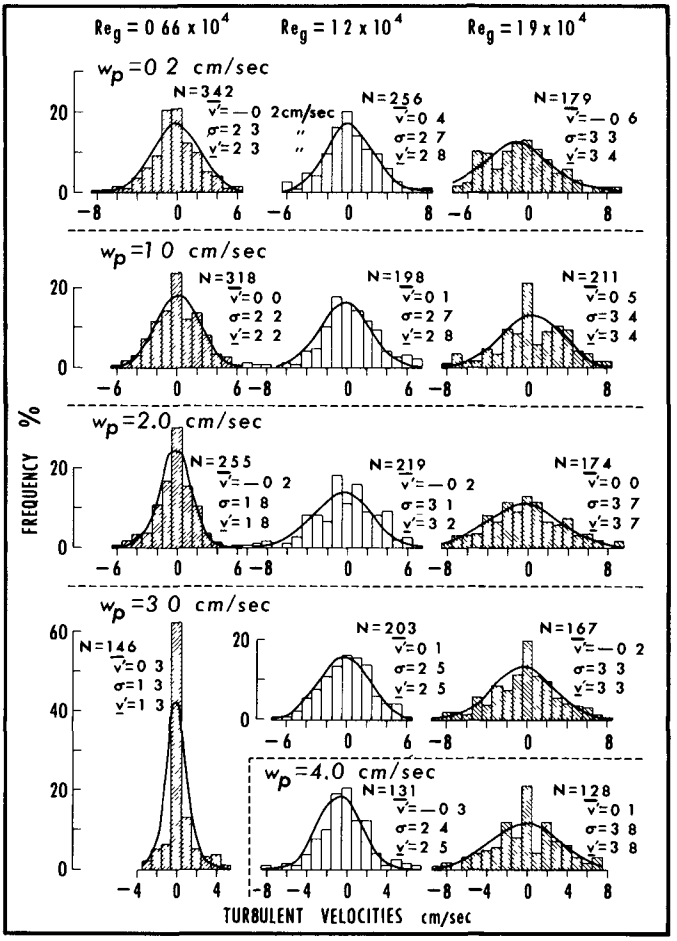

Fig. 3. Distributions of turbulent velocities v' as functions of grid Reynolds number Re_g, and particle fall velocity w_p.

3. The subscript y will hereafter be omitted and understood unless otherwise noted.

Much previous work suggests that the distribution of the fluid turbulence

should be Gaussian, and our data (w_p = 0.2 cm/sec) agree quite well. Liu (1956) states that the heavy particle turbulent velocities should also be Gaussian in distribution, which our present data likewise corroborate. Since the observations that make up any single velocity frequency distribution are scattered in time and space from many flow realizations, they lend strong support to the assumptions of long-term stationarity and homogeneity of the flow.

From elementary statistics we know the variance σ^2 of a quantity v'

$$\sigma^2(v') = \overline{(v'^2)} - \overline{(v')}^2, \tag{19}$$

or, transposing and taking roots,

$$\underline{v}' = \left[\sigma^2(v') + \overline{(v')}^2\right]^{1/2}. \tag{20}$$

Thus the intensity of turbulence $\underline{v}'$ may be evaluated directly from the variance and mean of our velocity frequency distributions. For a zero mean the intensity of turbulence is by definition equal to the standard deviation. Values of the mean $\overline{(v')}$, the standard deviation (σ), and intensity of turbulence ($\underline{v}'$) are given in Figure 3. Velocity means as anticipated are close to zero and show no preferential direction, supporting the absence of a mean flow.

Values of $\underline{v}'$ are presented in Figure 4 as a function of Re_g and w_p. For all values of w_p, higher grid Reynolds numbers produce higher intensities of turbulence. If $w_p >> 0$ then $v' \to 0$, since a particle with sufficient mass will not respond to even the highest fluid velocity fluctuations. At $Re_g = 0.66 \times 10^4$, $\underline{v}'$ apparently decreases monotonically with increasing values of w_p, but at higher grid Reynolds numbers a tendency is evident for an initial increase in $\underline{v}'$ before the descent to zero begins. These enhanced velocities are perhaps the result of centripetal accelerations; that is, the heavy particles are unable to maintain the rate of curvature of the fluid eddy and so are thrown from the eddy. This tendency decreases as the relative inertia increases, as postulated by Singamsetti (1966).

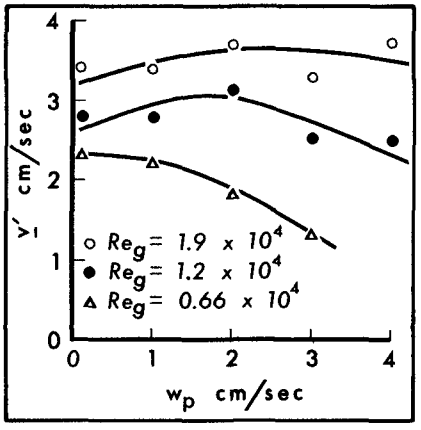

Fig. 4. The effect of the particle fall velocity w_p on the turbulence intensity $\underline{v}'$ for the three grid Reynolds numbers Re_g.

The ratio $w_p/\underline{w}_o$ was suggested by Rouse (1939) as a possible control on the mixing coefficient. Figure 5 is a nondimensional plot of $\underline{v}'/w_p$ against $w_p/\underline{w}'_o$ where $\underline{w}'_o$ is the fluid intensity of turbulence in the direction of fall.

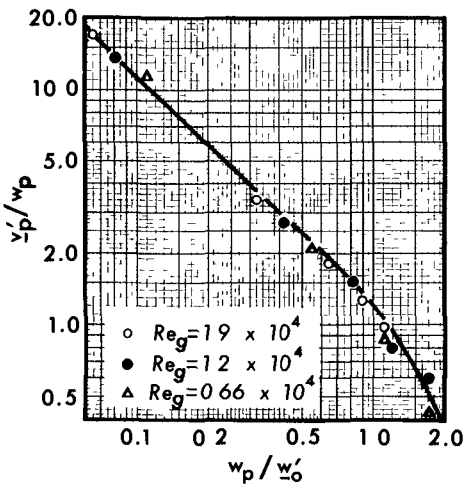

Fig. 5. Nondimensional representation of the effect of the particle fall velocity on the turbulence intensity.

The points of Figure 4 now fall on a single smooth curve. This curve can predict the horizontal turbulence intensity of the particle phase from that of the vertical fluid phase for a given particle fall velocity. This curve suggests that the initial increase in v'_p with increasing w_p is now present to some degree for all values of v'_o. The critical value of w_p/w'_o, computed from Figure 5, where v'_p begins to decrease (that is, where gravitational forces become dominant over inertial forces), varies $.7 < w_p/w'_o < .9$ as a function of w'_o. The onset of dominant particle gravitational effects is therefore not controlled by a critical particle Reynolds number as suggested for investigation by Rouse (1939).

In our quasi-isotropic flow field there is, of course, an intimate relation between w'_o and v'_o. Substitution of v'_o for w'_o in the abscissa variable of Figure 5 gives a very similar curve but with a little more scatter. Future work in a non-isotropic fluid must decide which of the two turbulence intensity components is the real controlling factor.

Other Fluid Turbulence Characteristics

Using our measured values of the time change of variance $d\sigma_o^2/dt$ (Table 2) and fluid turbulence intensity v'_o (Table 3) we can calculate other fluid properties such as scale time ($c \equiv t_o^*$) from (6), scale length ℓ_o^* from (9), diffusion coefficient K_o^* from (10), and the location of the mode of the Lagrangian power spectrum n_o from (11). These four quantities, together with the fluid turbulence intensity and energy per unit volume, are presented as a function of grid Reynolds number Re_g in Figure 6. As shown in (12), the scale time t^* can be interpreted in terms of the location of the mode of the Lagrangian power spectrum. In this regard it is generally found (see, e.g., Taylor, 1939) that the turbulence generated by grids at low values of Re_g is deficient in small-scale eddies; that is, the energy is concentrated at low frequencies. Increase of the grid Reynolds number should result in the production of relatively more high-frequency energy, producing a corresponding shift of the spectral mode toward high frequencies. This effect is seen both in the present study (Figure 6 C, D) and in that of Frenzen (1963) for the initial increase in grid Reynolds number. Our increase in the frequency of the spectral mode is evidently so severe as to force a slight increase in the diffusion coefficient K_o^* since, combining (10) and (11),

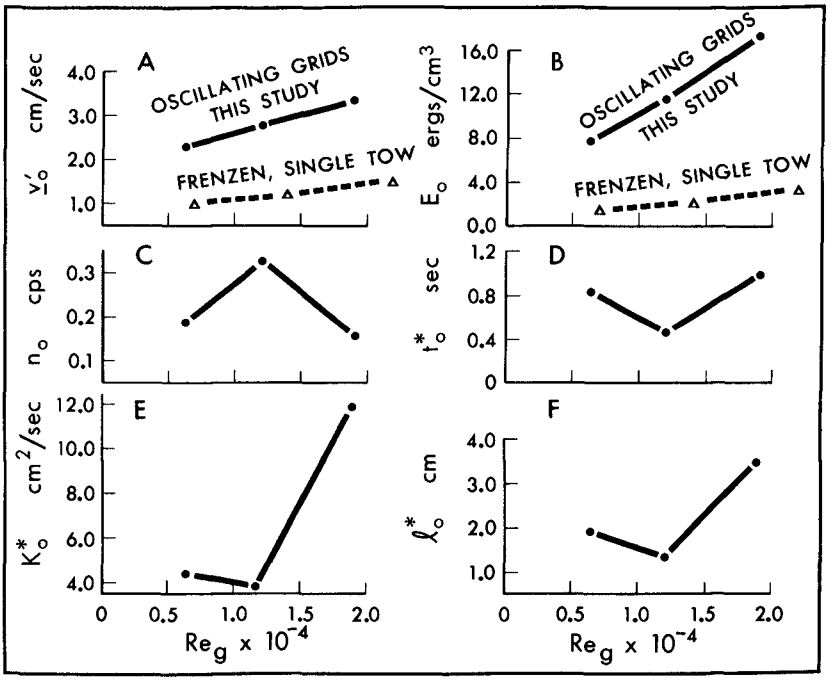

Fig. 6. Properties of the fluid turbulence produced by moving grids.

$$K_o^* = (\underline{v}')^2/2\pi n_o. \tag{21}$$

Taylor (1935) showed the energy of turbulence E_o per unit volume of fluid to be

$$E_o = \frac{\rho}{2}(3\underline{v}'^2_o). \tag{22}$$

Figure 6 B demonstrates that there is considerably more energy produced by the oscillating grids (this study) than by the single pass of a solitary grid (Frenzen). If the first increase in Re_g has excited considerable high-frequency energy, a further increase in the grid Reynolds number could conceivably be unable to shift the spectral mode any higher. In fact, owing to the overall increase in energy over the entire spectrum, the peak could shift back again toward lower frequencies, as suggested by Frenzen (1963) in a slightly different context. This did not, as a rule, occur in Frenzen's experiments but, as seen in Figure 6 B, at the highest grid Reynolds number we have considerably

Table 3
Characteristics of Fluid and Particle Turbulence

Re_g	0.66×10^4			
w_p cm/sec	0.2	1.0	2.0	3.0
$\underline{v}'$ cm/sec	2.3	2.2	1.8	1.3
t^* sec	.83	.49	0.77	1.3
ℓ^* cm	1.91	1.1	1.4	1.7
K^* cm^2/sec	4.4	2.4	2.5	2.2
n cps	.19	.32	.21	.12

Re_g	1.2×10^4				
w_p cm/sec	0.2	1.0	2.0	3.0	4.0
$\underline{v}'$ cm/sec	2.8	2.8	3.2	2.5	2.5
t^* sec	0.48	1.1	.78	0.59	.77
ℓ^* cm	1.4	3.2	2.5	1.5	1.9
K^* cm^2/sec	3.8	9.0	8.0	3.7	4.8
n cps	.33	.14	.20	.27	.21

Re_g	1.9×10^4				
w_p cm/sec	0.2	1.0	2.0	3.0	4.0
$\underline{v}'$ cm/sec	3.4	3.4	3.7	3.3	3.8
t^* sec	1.0	.95	.66	.64	.76
ℓ^* cm	3.5	3.2	2.4	2.1	2.9
K^* cm^2/sec	12	11	9.0	7.0	11
n cps	.16	.17	.24	.25	.21

more energy than he did--17 ergs/cm^3 as against 3.4 ergs/cm^3. This is likely the cause of the decrease in the frequency of the spectral mode n_o, the increase in the scale time t_o^*, and the corresponding sharp increase in the

diffusion coefficient K_o^* at the high value of Re_g. The scale length ℓ_o^* follows the same trend as the scale time t_o^*.

The relative particle diffusivity--that is, the ratio of the particle diffusion coefficient to that of the fluid K_p^*/K_o^*--is presented in Figure 7 as a function of particle fall velocity and grid Reynolds number. For the lowest and highest values of Re_g the relative diffusivity decreases fairly regularly with increasing particle fall velocity. For the middle value of Re_g there is a sharp increase in the relative diffusion, three out of four heavy particles diffusing at a higher rate than the fluid (quasi-neutral) particles. As can be seen in Table 3, this relative diffusion peak is entirely the result of the unexpectedly low value of the fluid diffusion coefficient (w_p = 0.2 cm/sec) at the intermediate grid Reynolds number $Re_g = 1.2 \times 10^4$. To add to our suspicion of this value, the heavy particle diffusion coefficients at this grid Reynolds number have values which are fairly consistent with the two other data sets.

Nonetheless, a detailed recheck of the raw data revealed no errors in the analysis. In its support it should be noted that the diffusion coefficient is directly measured (not computed) from the time change of particle displacement; as such it is based on approximately 150 points. Furthermore, the turbulent velocity frequency distribution of w_p = 0.2 cm/sec at $Re_g = 1.2 \times 10^4$, which is based on the same raw data as the diffusion coefficient in question, is very well behaved. This distribution (cf. Fig. 3) fits a Gaussian curve extremely well and has a standard deviation (intensity of turbulence) falling midway between those of neighboring Reynolds numbers. Thus the relative diffusion anomaly is apparently quite real and must be related to shifts in the power spectra along the frequency axis, as discussed earlier (cf. equation 21). The unresolved question is why at the intermediate Re_g there is a lack of coupling between the fluid and the heavy particles with respect to diffusion, but coupling with respect to particle velocity.

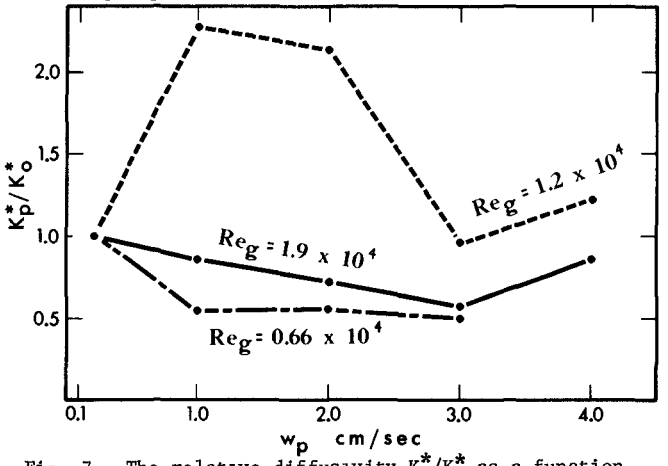

Fig. 7. The relative diffusivity K_p^*/K_o^* as a function of the particle fall velocity w_p.

It is generally believed that the more turbulent the flow the higher the degree of mixing (diffusion) of such properties as heat, momentum, sediment, aerosols, etc. Despite the relative diffusion anomaly in our data, this tendency is still clearly shown for our experiments in Figure 8, even allowing for scatter caused by varying particle fall velocity. There is also some evidence for a correlation (see Figure 9) between relative

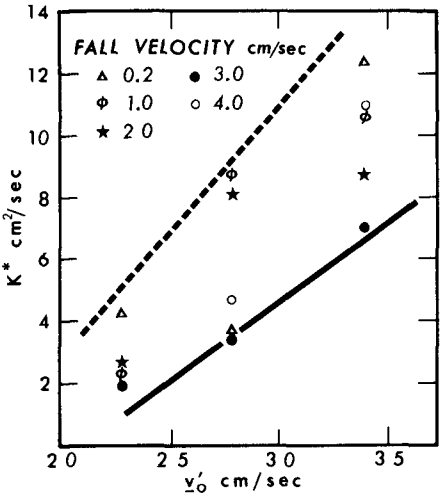

Fig. 8. The effect of the fluid turbulence intensity on the diffusion coefficients.

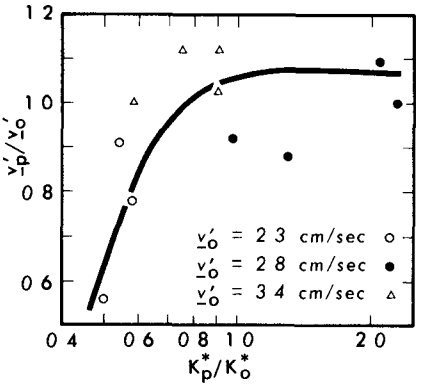

Fig. 9. The relative diffusion coefficient as a function of relative particle velocity.

particle velocity $\underline{v}_p'/\underline{v}_o'$ and relative particle diffusivity K_p^*/K_o^*. The rate of increase of the relative particle diffusivity accelerates greatly after the ratio $\underline{v}_p'/\underline{v}_o'$ exceeds approximately unity.

The particle turbulence intensity $\underline{v}_p'$ is equal to the ratio of the scale length ℓ_p^* and the scale time t_p^*

$$\underline{v}_p' = \ell_p^*/t_p^*. \tag{23}$$

It is of interest to investigate the interrelation of these three quantities. Figure 10 shows that the particle scale length (average eddy size) increases with increasing particle turbulence intensity, but with appreciable scatter because of fall velocities and frequency shifts in the power spectra. With this constraint as particle turbulence intensity increases, the scale time may then either be a constant or increase at various rates. A plot of our data is inconclusive as to the behavior of t_p^* with $\underline{v}_p$, except that t_p^* is not a constant. Apparently, fall velocity effects, power spectra shifts, and other unknown interactions control the particle scale time. This conclusion applies also to the frequency of the peak of the particle power spectrum n_p.

The frequency of the power spectral modes, both fluid and particle phases, do, however, fall in the range predicted by (16) as available to our observation.

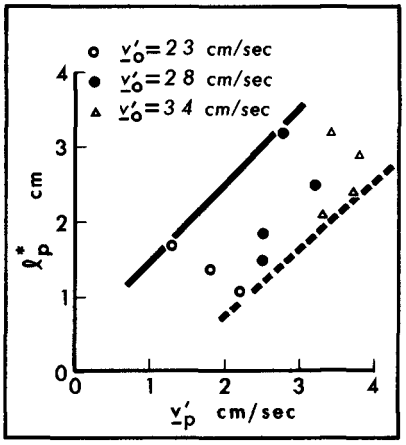

Fig. 10. The Lagrangian heavy particle length scale ℓ^*_p as a function of the turbulence intensity.

Further Discussion

All of the results up to this point have been independent of any assumption concerning the nature of the Lagrangian autocorrelation function. If we assume the often observed negative exponential shape for this function the general diffusion equation (14) results. Through (11) this equation could be written directly in terms of our measured quantities $\underline{v}'$ and K^*. Figure 11 shows a selection of the theoretical relations predicted by (14)--using our measured values of $\underline{v}'$ and K^*--compared to the experimentally observed values of particle variance σ^2 at a given time t. In general, the agreement is good. Part of the agreement is forced, of course, since the linear slope of the solid lines is computed from the observed points, but the line itself is free to wander in the σ^2-t plane. Certain systematic deviations of the observed values from the theoretical predictions (such as $Re_g = 1.2 \times 10^4$, $w_p = 2.0$ cm/sec in Figure 11) are perhaps caused by the fact that the heavy particle autocorrelation functions do not follow the exponential decay rule. This general agreement, however, supports the application of the Taylor diffusion theory to heavy particles.

A further check on the suitability of the Taylor theory can be made starting from (13). The exponential term is negligible after 2 seconds. By rearranging the remaining terms on the right hand side into the slope-abscissa intercept form of the linear equation, it is seen that the abscissa intercept of the linear portion of the σ^2-t curve is equal to the scale time t^*. Using (11) and the measured values of K^*, it is now possible to calculate values of the turbulence intensity. These are compared to the experimentally observed values in Table 4.

Table 4
Value of Turbulence Intensity cm/sec

$Re_g \times 10^{-4}$	0.66				1.2					1.9				
w_p *	.2	1	2	3	.2	1.0	2.0	3.0	4.0	.2	1	2	3	4
$\underline{v}'$ Obs. *	2.3	2.2	1.8	1.3	2.8	2.8	3.2	2.5	2.5	3.4	3.4	3.7	3.3	3.8
$\underline{v}'$ Calcu.*	2.5	2.8	3.6	1.5	3.4	2.6	2.7	1.8	3.2	2.9	2.8	6.1	11	4.0

* cm/sec

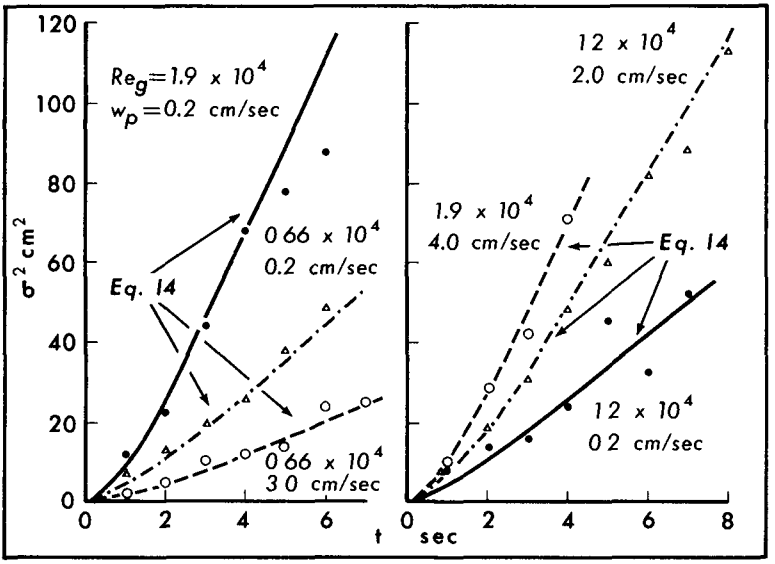

Fig. 11. A selection of experimental data on the time change of the variance of particle displacements σ^2 compared to a form of the Taylor diffusion equation.

The average error for the fourteen observations is $\pm$23 percent, which is not unreasonable considering the large error in t^* and $\underline{v}'$ produced by a relatively small error in the linear slope of the σ^2-t curve. Orlob (1959) describes yet another method of calculating diffusion parameters from particle spread.

V. SUMMARY AND CONCLUSIONS

The turbulent diffusion of quasi-neutral and heavy particles is studied in a turbulence field generated by an array of oscillating grids. Particle displacements caused by turbulence are measured by means of multiple-image photography. Diffusion coefficients and intensities of turbulence are directly measured from the photographic data. Other turbulence parameters can then be calculated.

The principal conclusions concerning the horizontal component of the turbulence are as follows:

(1) The simple experimental technique of oscillating an array of grids at various speeds produces turbulent fields with suffi-

cient homogeneity and stationarity to permit accurate study of heavy particle diffusion.

(2) The turbulent velocity distributions of both the fluid (quasi-neutral particles) and the heavy particles are Gaussian, with no evidence of a mean flow.

(3) The turbulent intensity of the heavy particle phase is closely controlled by the particle fall velocity and the fluid turbulent intensity in the vertical direction. Gravitational effects begin to dominate the heavy particle turbulence intensity after $w_p/\underline{w}_o'$ exceeds approximately 0.8.

(4) Taylor's statistical theory of turbulence effectively describes the horizontal diffusion of heavy particles suspended in a fluid.

(5) In general, the heavy particle diffusion coefficients and the scale length of the particle eddies increase with increasing fluid turbulent intensity.

(6) Relative diffusion (ratio of heavy particle diffusivity to fluid diffusivity) is a function of particle fall velocity and internal characteristics of the turbulence such as frequency shifts in the power spectra. This suggests that the turbulence spectrum as well as the orbital velocities may exert control on grain diffusion by waves.

ACKNOWLEDGMENTS

The experimental portion of this study was conducted in the Fluid Mechanics Laboratory of the Delft Technological University under a National Science Foundation Postdoctoral Fellowship.

Further support enabling the detailed data analysis and manuscript preparation was provided by the Coastal Studies Institute under the sponsorship of the Office of Naval Research, Geography Branch, Contract No. Nonr 1575(03), NR 388 002. Hyuck J. Kwon of the Institute was especially valuable in the data analysis.

NOTATION

c	the area under the autocorrelation curve
d	the diameter of the test particles (2mm)
d_s	the sedimentation diameter
E	the energy of the turbulence
K^*	the diffusion coefficient
ℓ^*	the scale length of the turbulence
M	the grid mesh length
n	the frequency of the power spectrum mode or the number of observations
N	the number of observations
Re_g	the grid Reynolds number
Re_p	the particle Reynolds number
t, T	time
t^*	the scale time of the turbulence
$\bar{U}$	the mean horizontal velocity, or its experimental equivalent the average speed of the sinusoidal grid motion
u', v', w'	turbulent velocity in the x, y, or z direction
$\overline{(v'^2)}^{1/2}$, $\underline{v}'$	the turbulence intensity in the y direction
w_p	the terminal fall velocity of a particle in still water
$\underline{w}'_o$	the fluid turbulence intensity in the vertical direction
x, y, z	the direction, respectively, of the grid motion, horizontal across the grid motion, in the vertical
ν	the kinematic viscosity
ξ	the autocorrelation lag time
ρ	the fluid density
σ^2	the statistical variance of a quantity
$( )_o$	the subscript refers to fluid or quasi-neutral particle or to initial particle position
$( )_p$	the subscript refers to a heavy particle

References

Bowen, A. J. and D. L. Inman, 1966, Budget of littoral sands in the vicinity of Point Arguello, California. Tech. Memo. No. 19, Coast. Eng. Res. Center, Corps of Eng., 41 pp.

Brown, C. B., 1950, Sediment transportation. In (H. Rouse, ed.) Engineering hydraulics. New York (J. Wiley & Sons), pp. 769-855.

Frenzen, P., 1963, A laboratory investigation of the Lagrangian autocorrelation function in a stratified fluid. Argonne National Lab. Rept. 6794, 168 pp.

Haltiner, G. J. and F. L. Martin, 1957, Dynamical and physical meteorology. New York (McGraw-Hill Book Co., Inc.), 470 pp.

Inoue, E., 1951, On the Lagrangian correlation coefficient for turbulent diffusion and its application to atmospheric diffusion phenomena. In Geophys. Res. Pap. No. 19, Geophys. Res. Dir., A.F.C.R.C., Cambridge, Mass., 530 pp.

Inoue, E., 1960, On the shape of stack plumes. Mem. on Meteor. Res., Jap. Met. Soc., 11:332-339.

Kalinske, A. A. and C. L. Pien, 1944, Eddy diffusion. Ind. Eng. Chem., 36:220-223.

Liu, V. C., 1956, Turbulent dispersion of dynamic particles. Jour. of Meteorology, 13, No. 4, pp. 399-405.

Murray, S. P., 1967, Control of grain dispersion by particle size and wave state. Jour. Geol., 75, No. 5, pp. 612-634.

Orlob, G. T., 1959, Eddy diffusion in homogeneous turbulence. Proc. A.S.C.E., 85, No. HY 9, pp. 75-101.

Prandtl, L., 1939, Beitrag zum turbulenz symposium. Proc. 5th Inter. Cong. App. Mech., pp. 340-346.

Rouse, H., 1939, Experiments on the mechanics of sediment suspension. Proc., 5th Inter. Cong. App. Mech., pp. 550-554.

Singamsetti, S. R., 1966, Diffusion of sediment in a submerged jet. Jour. of the Hydraulics Div., A.S.C.E., No. HY 2, pp. 153-168.

Stewart, R. W. and H. L. Grant, 1962, Determination of the rate of dissipation of turbulent energy near the sea surface in the presence of waves. Jour. Geophys. Res., v. 67, no. 8, pp. 3177-3180.

Sutton, O. G., 1953, Micrometeorology. New York (McGraw-Hill Book Co., Inc.), 333 pp.

Taylor, G. I., 1921, Diffusion by continuous movements. Proc. Lon. Math. Soc., 20:196 -212.

Taylor, G. I., 1935, Statistical theory of turbulence. Parts I-IV, Proc. Roy. Soc. Lon., A151, pp. 421-478.

Taylor, G. I., 1938, The spectrum of turbulence. Proc. Roy. Soc. Lon., A164, pp. 476-490.

Taylor, G. I., 1939, Some recent developments in the study of turbulence. Proc. 5th Inter. Cong. App. Mech., pp. 294-310.